Japanese-German Spring School

on solidification and phase transformation

March 30th and 31st, 2022

Prof. Manja Krüger

Prof. Kyosuke Yoshimi

Program

March 30th, 2022

Zoom-Meeting
https://us02web.zoom.us/j/89173001669

Meeting-ID: 891 7300 1669

Jap	Ger	
17^{00}	09^{00}	**Welcome notes**
17^{10}	09^{10}	**Rachid Stefan Touzani** How to use density functional theory to study phase transitions - problems and possibilities -
17^{30}	09^{30}	**Julia Becker** Properties of density optimized Mo-Si-B alloys
17^{50}	10^{50}	**Georg Hasemann** Microstructure evolution and ternary eutectic reaction in the V-Si-B system
18^{10}	10^{10}	**Janett Schmelzer** V-Si-B: Ways of improving high-temperature strength and oxidation resistance
18^{30}	10^{30}	**Discussion and remarks**
19^{00}	11^{00}	**End of the first session**

Program

March 31st, 2022

Zoom-Meeting
https://us02web.zoom.us/j/89173001669

Meeting-ID: 891 7300 1669

Jap	Ger	
17^{00}	09^{00}	**Maximilian Regenberg** Further development of a novel Ta-Nb-Ti multi-component alloy for biomedical applications
17^{20}	10^{20}	**Rostyslav Nizinkovskyi** A numerical efficient non-local Allen-Cahn model for estimation of equilibrium morphology of constrained precipitates
17^{40}	09^{40}	**Shuntaro Ida** Solidification pathway and microstructure of TiC in Mo-Si-B-, Mo- and Fe-based alloys
18^{00}	10^{00}	**Naoma Abe** Microstructure and material properties of rapidly-solidified MoSiBTiC alloy
18^{20}	10^{20}	**Xinyu Yan** Microstructure evolution through solidification of Cr and Nb-added MoSiBZrC alloy
18^{40}	10^{40}	**Discussion and remarks**
19^{00}	11^{00}	**End of the second session**
20^{00}	12^{00}	**Online Spring School party** Our virtual social event. Cheering, laughing, sharing drinks and toasts

Further development of a novel Ta-Nb-Ti multi-component alloy for biomedical applications

Maximilian Regenberg[1], Janett Schmelzer[1], Georg Hasemann[1], Jessica Bertrand[2] and Manja Krüger[1]

[1] Institute of Materials and Joining Technology, Otto-von-Guericke University Magdeburg, Universitätsplatz 2, 39106 Magdeburg, Germany
[2] Department of Orthopedic Surgery, Otto-von-Guericke University Magdeburg, Leipziger Str. 44, 39120 Magdeburg, Germany

The modern material class of equiatomic multi-component alloys, especially high-entropy alloys (HEAs) gained tremendous attention in the scientific community over recent years, which can be attributed to two main reasons: Firstly, the new concept of combining several elements (at least 5 principal elements with concentrations between 5 and 35 at. % [1]) in contrast to conventional alloys, mostly containing only two or three elements in addition to the main alloy constituent. This results in a broad variety of possible combinations thus leading to completely novel alloys with exceptional properties. Secondly, recently developed refractory metal based high-entropy alloys (RHEAs) have shown properties that are superior to the ones of current state-of-the-art alloys, which are attributed to several unique thermodynamic effects [2,3]. However, besides the outstanding mechanical properties, abrasion resistance and thermal resistance, a vast variety of chemical elements used in RHEAs also belong to the category of biocompatible elements, hence leading to potentially new biomedical materials.

To meet the demands for biomedical applications, specifically for implant materials, three main criteria must be fulfilled: Excellent mechanical properties (regarding the force transmission between implant and bone), corrosion resistance (prevention of corrosive damage to the implant) and biocompatibility (no tissue damage by the implant material or by corrosive/ abrasive particles) [1]. The present study meets these targets on the basis of previous investigations regarding Mo-Nb-V-W-Ti high-entropy alloys [2], which have confirmed promising mechanical properties. Furthermore, the works of Shi et al. [3], Shittu et al. [4] and Yuan et al. [5], concerning the corrosive capabilities and degradation resistance, as well as the biocompatibility of HEAs, are considered to support our theories. However, in consideration of this background and due to the excellent biocompatibility of the constituents [6], an equiatomic composition of Ta, Nb and Ti as multi-component base alloy was chosen for the experiments.

The alloy examined was produced using an arc melting furnace under Ar atmosphere, metallographically prepared and investigated respectively. Scanning electron microscopy (SEM) analysis revealed the presence of a dendritic microstructure, with an enrichment of high-melting elements in the dendrites, as well as Ti in the interdendritic regions (verified by means of EDS mappings). Microstructure analysis by means of X-ray diffraction (XRD) showed, that there are two types of body-centered cubic (bcc) crystal structures (Im-3m I: a = 3.287 Å; Im-3m: a = 3.291 Å) present in the as-cast state. To get a better understanding of the microstructure evolution, heat-treatment experiments regarding different temperatures and times were performed. Furthermore, the alloy produced, as well as samples of elemental Ta, Nb, alloy Co-28Cr-6Mo and alloy Ti-6Al-4V, were prepared to a defined surface grade. The topography of the surfaces was evaluated using confocal microscopy and contact angle measurements subsequently. Afterwards, the biocompatibility of the novel alloy Ta-Nb-Ti was evaluated by means of cell (osteoblasts) attachment (depicted in the Figure**Fehler! Verweisquelle konnte nicht gefunden werden.**), as well as monocyte inflammatory response analysis. First results indicate competitive osteoblast attachment, as well as comparable expressions of fibrosis markers in comparison to conventionally used biomedical materials. In addition, the Ta-Nb-Ti alloy showed a markedly reduced inflammatory capacity, indicating a high potential for use as prospective biomedical material.

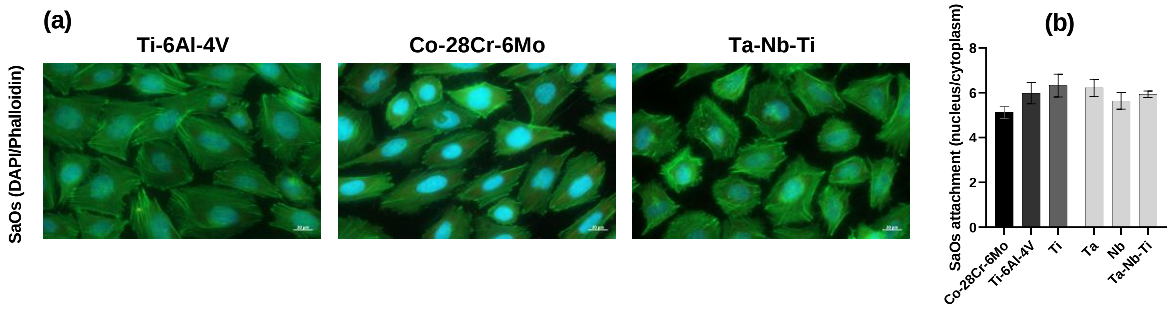

(a) Osteoblast attachment to the surface of alloy Ti-6Al-4V, alloy Co-28Cr-6Mo and novel alloy Ta-Nb-Ti. (b) assessment of nucleus/cytoplasm ratio of the osteoblasts on novel alloy Ta-Nb-Ti, compared to reference samples.

References

[1] Houis, S.; U.a. Medizintechnik; Wintermantel, E., Ha, S.-W., Eds.; Springer Berlin Heidelberg: Berlin, Heidelberg, 2009; ISBN 978-3-540-93935-1.
[2] Regenberg, M.; Hasemann, G.; Wilke, M.; Halle, T.; Krüger, M. Microstructure Evolution and Mechanical Properties of Refractory Mo-Nb-V-W-Ti High-Entropy Alloys. Metals (Basel). 2020, 10, 1530.
[3] Shi, Y.; Yang, B.; Liaw, P.K. Corrosion-resistant high-entropy alloys: A review. Metals (Basel). 2017, 7, 1–18.
[4] Shittu, J.; Pole, M.; Cockerill, I.; Sadeghilaridjani, M.; Reddy, L.V.K.; Manivasagam, G.; Singh, H.; Grewal, H.S.; Arora, H.S.; Mukherjee, S. Biocompatible High Entropy Alloys with Excellent Degradation Resistance in a Simulated Physiological Environment. ACS Appl. Bio Mater. 2020, 3, 8890–8900.
[5] Yuan, Y.; Wu, Y.; Yang, Z.; Liang, X.; Lei, Z.; Huang, H.; Wang, H.; Liu, X.; An, K.; Wu, W.; et al. Formation, structure and properties of biocompatible TiZrHfNbTa high-entropy alloys. Mater. Res. Lett. 2019, 7, 225–231.
[6] Andersen, P.J. Metals for use in medicine; Elsevier Ltd., 2017; Vol. 1; ISBN 9780081006924.

A numerical efficient non-local Allen-Cahn model for estimation of equilibrium morphology of constrained precipitates

Rostyslav Nizinkovskyi

Crystallographic eigenstrains play a crucial role in almost every aspect of the solid-solid phase transformations. The character of the eigenstrains affects amongst other the morphology of product phase. In this scope, the newly developed multiphase model for morphology estimation is presented. Qualitative and quantitative comparison with models, available in literature, is done.

The model predictions for the Fe-Cu system are discussed in scope of available experimental data and classic crystallographic models. The morphology of the precipitate is found to qualitatively agree with recent APT data, HRTEM studies and theoretic predictions. In spite of the qualitative agreement, the length-to-width ratio deviates significantly from experimental observations. The reasons for this discrepancy are analyzed with the simulations. Finally, the simulation of twinned precipitate is done to analyze the role of coherent twins on nanostructure formation.

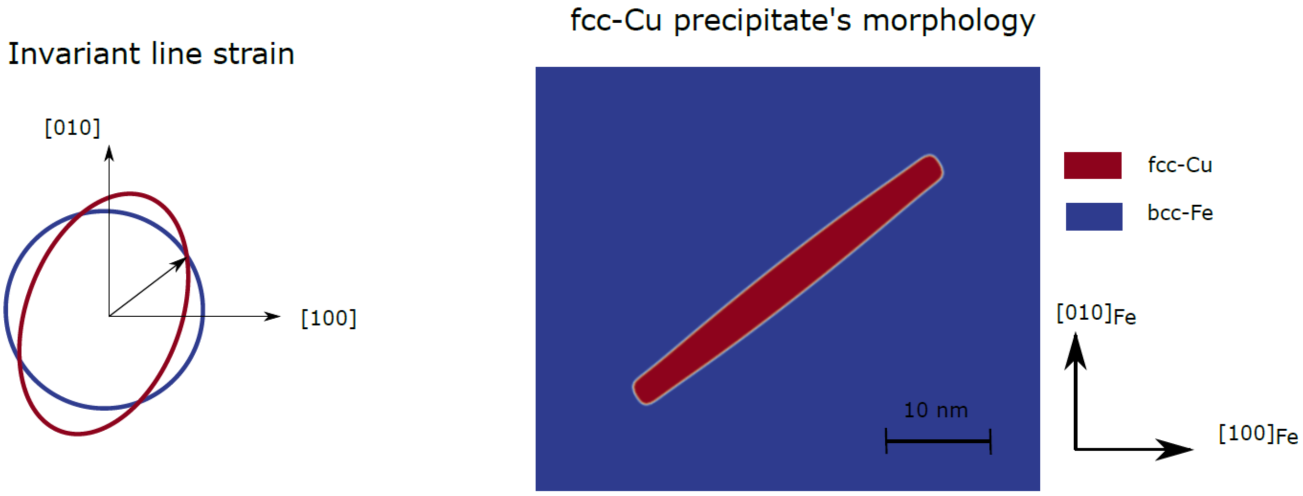

Interrelation of the invariant line strain and fcc-Cu precipitate’s morphology [1]

References

[1] Nizinkovskyi, Rostyslav. Study of the formation of ellipsoidal precipitates in Fe-Cu alloys via phase-field method. Preprint under consideration in Journal of Nuclear Materials

How to use Density Functional Theory to study phase transitions – Problems and possibilities

Rachid Stefan Touzani

Institute of Materials and Joining Technology, Otto-von-Guericke University Magdeburg

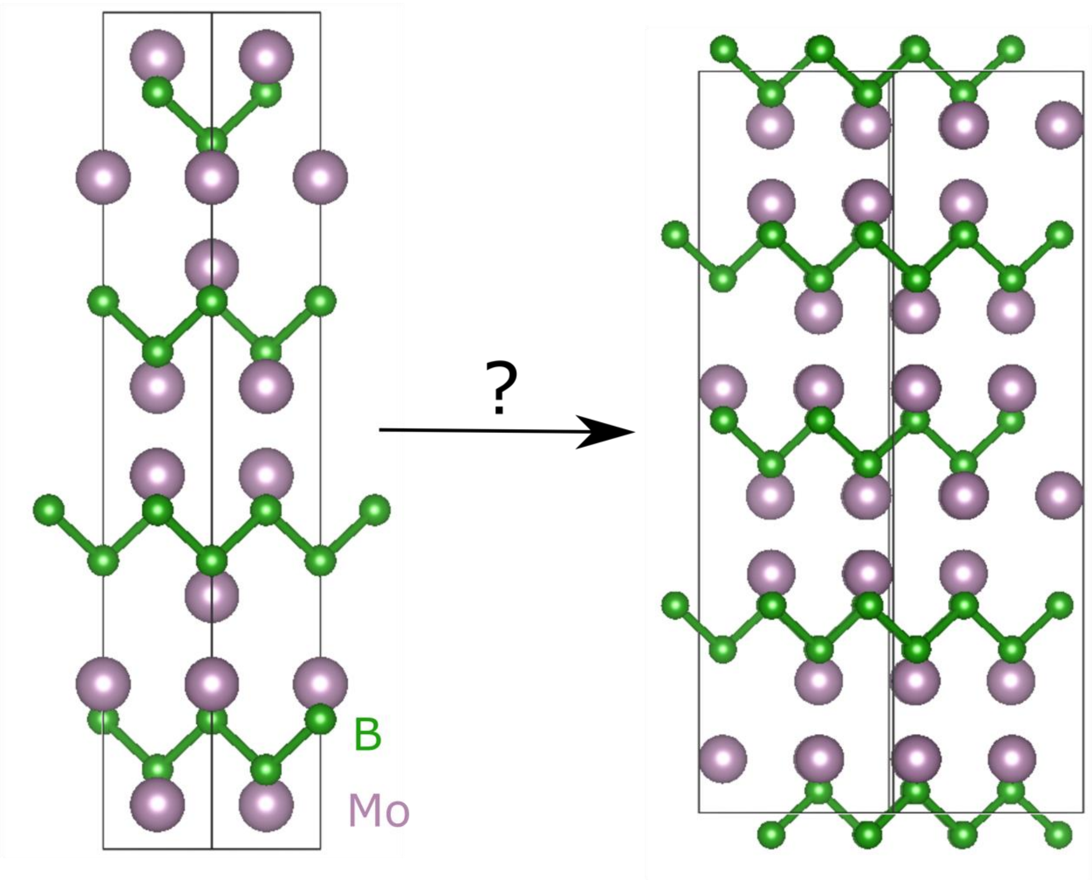

Crystal structures of α-MoB (left) and β-MoB (right)

Per se, in Density Functional Theory (DFT) the ground state electron density is used and therefore DFT is usually only able to predict and explain ground state properties of atoms, molecules and solids which are at 0 K and 0 bar. Phase transitions, however, take place at higher temperatures and/or higher pressure, so at first glance DFT is not able to predict phase transitions. Luckily, the derivatives of the ground state energy and the usage of several thermodynamic statistics can be used to model phase transitions in the solid phase quite straightforward. In my talk, I will give the insights of how phase transitions can be investigated using DFT and show as an example the phase transition of α-MoB to β-MoB.

Properties of density optimized Mo-Si-B alloys

Julia Becker

Improving the efficiency of turbines for power plants and aircraft engines is an increasingly important research subject. Ternary Mo-Si-B alloys, consisting of a molybdenum solid solution (Mo_{ss}) phase and two intermetallic phases Mo_5SiB_2 (T2) and Mo_3Si, are able to combine balanced room temperature fracture toughness, high temperature creep strength and good oxidation performance. However, the high density (> 9 g cm^3) of this class of alloys is a drawback when used as a turbine blade material. Therefore, the present thesis deals with vanadium as a potential alloying partner for density optimized Mo-based alloys. Different alloy compositions Mo-xV-Si-8B (x = 10, 20, 30, 40 at.%) were produced by powder metallurgy, including mechanically alloying and a thermal treatment, to observe the effects of V as a solute in the respective phases. The thermomechanical characterization was carried out on sintered (FAST) and arc-melted Mo-40V-9Si-8B alloys. Three point-bending with notched samples as well as compressive creep tests reveal a high fracture toughness and acceptable creep strength of this new type of alloys. Furthermore, the effect of minor additions of Fe on the oxidation resistance was investigated by cyclic oxidation tests.

Microstructure Evolution and Ternary Eutectic Reaction in the V-Si-B System

Georg Hasemann[1] and Weiguang Yang[2]

[1] Otto-von-Guericke University Magdeburg, Institute of Materials and Joining Technology, Universitätsplatz 2, 39106 Magdeburg, Germany

[2] Forschungszentrum Jülich GmbH, Institute of Energy and Climate Research, Microstructure and Properties of Materials (IEK-2), Leo-Brand-Str. 1, 52425 Jülich, Germany

The solidification behavior of arc-melted alloys in the V-rich portion of the ternary V-Si-B alloy system has been experimentally investigated. A detailed microstructure analysis of several as-cast alloys based on SEM observations, EDS/WDS and EBSD measurements was carried out. As a result, different solidification reactions in the V-rich V-Si-B system were identified. The new data allow a reconstruction of the liquidus surface of the V-Si-B phase diagram [1]. Furthermore, two different types of ternary eutectics were identified. By carrying out this wok, special attention was paid to the V_{SS}-V_3Si-V_5SiB_2 ternary eutectic. Different alloy compositions had been investigated experimentally to determine the chemical composition of this ternary eutectic reaction [2]. The V-based ternary eutectic is isomorph to the well-known Mo-Si-B system and the Mo_{SS}-Mo_3Si-Mo_5SiB_2 ternary eutectic. However, the V-based ternary eutectic has a solid solution character since V_{SS} forms the major phase as compared to the intermetallic character of the Mo-base eutectic with the Mo_3Si phase as the major phase. This will have advantages considering low temperature deformability and fracture toughness.

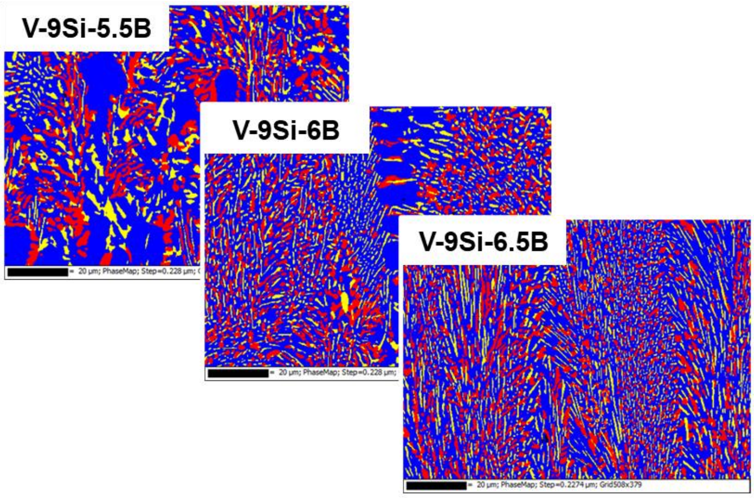

EBSD-images of eutectic formation

References

[1] G. Hasemann, Journal of Alloys and Compounds 824 (2020) 153843.

[2] W.G. Yang, G. Hasemann, M. Yazlak, B. Gorr, R. Schwaiger, M. Krüger, Journal of Alloys and Compounds 902 (2022) 163722.

V-Si-B: Ways of improving high-temperature strength and oxidation resistance

Janett Schmelzer, Silja-Katharina Rittinghaus, Marcel Giese, Hannes Eley and Manja Krüger

The presence of the vanadium solid solution phase is essential for the use of innovative V-Si-B structural materials in terms of processability, as it contributes in a significant manner the ductility of the material. Next to the strength silicide phases, a minimum of 30 vol. % of the ductile V solid solution (V_{ss}) phase is considered to be necessary in structural V-Si-B alloys. However, the solid solution phase is the weakest phase in terms of high-temperature strength and oxidation resistance. To allow vanadium alloys to be used at temperatures > 600 °C, innovative ways of improving high-temperature properties by means of microstructure-property-relationship resulting from different manufacturing processes and particle strengthening approaches are presented.

Solidification pathway and microstructure of TiC in Mo-Si-B-, Mo- and Fe-based alloys

Shuntaro Ida and Kyosuke Yoshimi

The solidification pathway of the TiC added Mo-Si-B based alloy (hereafter MoSiBTiC alloy) is rationalized based on the solidification pathway of Mo-Si-B ternary system [1-3]. In the Mo-5Si-10B-10Ti-10C (at%) alloy, the primary TiC phase is formed followed by Mo+TiC eutectic reaction before the peritectic reaction of Liquid+Mo_2B -> Mo+T_2 which is followed by the formation of primary Mo phase in the Mo-Si-B ternary system. This solidification path change is caused by the high melting point of TiC. Finally, two eutectic reactions occur: Liquid -> Mo+T_2+TiC and Liquid -> Mo+T_2+Mo_2C.

In the Mo-Ti-C ternary system in the Ti-poor region, the ternary peritectic reaction of L+Mo_2C -> Mo+TiC around Mo-18Ti-18C takes place and the eutectic reaction of L -> Mo+TiC occurs at a higher Ti content [4]. The solidified microstructure of TiC in the MoSiBTiC alloy is similar to that of the Mo-Ti-C ternary alloy and the primary TiC has a dendric shape and the interface between TiC and Mo phase of eutectic microstructure is curved.

The Fe-Ti-C ternary alloy also has the primary TiC and the eutectic microstructure of L -> γ-Fe+TiC. In the Fe-15Ti-15C (at%), the primary TiC has a dendric shape at the initial stage of solidification but the morphology changes to a cuboidal shape with decreasing temperature and/or solute elements in the liquid [5]. The Fe-5Ti-5C (at%) which has a lower liquidus temperature of TiC compared to Fe-15Ti-15C (at%) shows the primary TiC with a cuboidal shape with the $\{001\}_{TiC}$ habit planes (see Figure). The eutectic microstructure of TiC is also faceted and changing to a plate shape with the $\{011\}_{TiC}$ habit planes and a needle shape with the $[001]_{TiC}$ growth direction. The morphology of TiC might be determined by the anisotropy of the surface energy and the growth rate of TiC in the liquid. The cuboidal shape with the $\{001\}_{TiC}$ habit planes can be formed because of the minimum surface energy of the $\{001\}_{TiC}$. However, the plate shape TiC with the $\{011\}_{TiC}$ habit planes and the needle shape TiC with the $[001]_{TiC}$ growth direction exhibits the slowest growth rate of $\langle 011 \rangle_{TiC}$ and the fastest growth rate of $\langle 001 \rangle_{TiC}$, respectively.

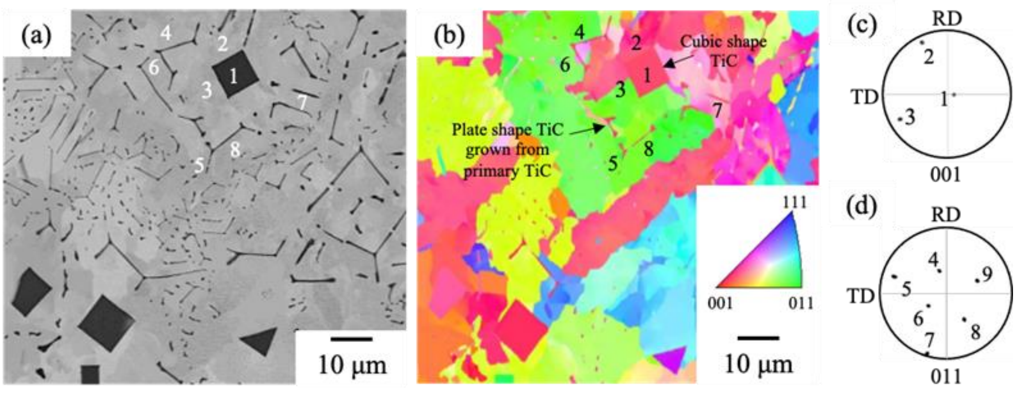

Microstructure and orientation of TiC in Fe-5Ti-5C (at%): (a) Backscattered electron image, (b) Inverse pole figure map of corresponding area of (a), (c) 001 pole figure of a cubic shape TiC, (d) 011 pole figure of a plate shape TiC. The numbers show habit plane of TiC: 1-3 are $[001]_{TiC}$ habit planes of a cubic shape TiC and 4-9 are the $\{011\}_{TiC}$ habit planes of plate shape TiCs.

References

[1] H. Fukuyama et al., SCIENTIFIC REPORT, 9, (2019), 15049.
[2] H. Fukuyama et al., Materialia, 13, (2020), 100867.
[3] G. Hasemann et al., Materials & Design, 185, (2020), 1082333.
[4] S. Ida et al., High Temperature Materials and Processes, 39, (2020), 164-170.
[5] S. Ida et al., Materialia, Under review.

Microstructure and Material Properties of Rapidly-Solidified MoSiBTiC Alloy

Naoma Abe, Kyosuke Yoshimi

Introduction: 1st generation MoSiBTiC alloy (65Mo-5Si-10B-10Ti-10C (at.%)) is one of the promising candidates for ultra-high temperature materials. On the other hand, this alloy suffers from hard-to-machining. To overcome this problem, the use of additive manufacturing (AM) is being considered. Since the cooling rate in AM process is extremely high, the microstructure of AMed alloy would be different from that of the alloy produced by traditional manufacturing processes. For this reason, it is greatly worth investigating the material properties of AMed MoSiBTiC alloy. However, it takes a long time to prepare such material because it is necessary to fabricate suitable powder and optimize process parameters for AM. Therefore, in this study, rapid solidification (RS) was focused on. Through this process, samples with fine microstructures that develops by AM can be easily simulated without the powder preparation and process parameter optimization. The objective of this study is to investigate the effect of microstructure refining on the material properties of the MoSiBTiC alloy by a RS process.

Experimental procedure: 1st generation MoSiBTiC alloy (65Mo-5Si-10B-10Ti-10C (at.%)) was made by two methods; arc-melting (As-cast sample) and tilt-casting which is one of the rapid solidification processes (RS sample). Isothermal oxidation tests at 800 and 1100°C for 24 h are conducted in $21O_2$-$79N_2$ (ml/min).

Result: RS sample had much finer microstructure than As-cast sample, which size was below sub-micron. Near the surfaces where the cooling rate is very fast, TiC, Mo_{ss}-TiC (eutectic), and Mo-Mo_5SiB_2 (eutectic) were mainly developed, while around the center where the cooling rate is slower than the surfaces but faster than the As-cast sample, Mo_{ss}-TiC-T_2-Mo_2C (eutectic) was mainly developed (see Figure). These phases were also observed in the As-cast sample. The oxidation resistance of the RS sample was well improved at 1100°C but worsened at 800°C.

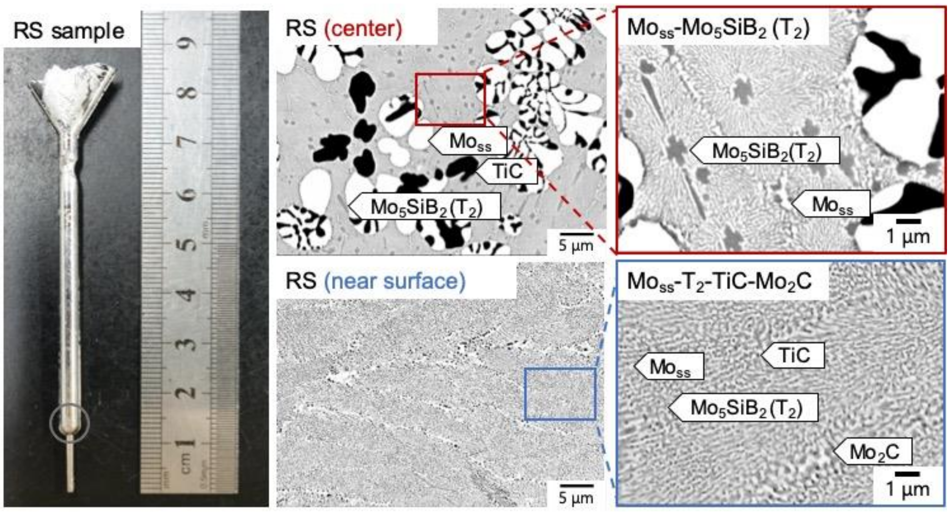

Microstructure of 1st generation MoSiBTiC alloy produced by the tilt-casting process.

Microstructure evolution through solidification of Cr and Nb-added MoSiBZrC alloy

Xinyu Yan, Xi Nan, Shuntaro Ida, and Kyosuke Yoshimi

As shown in the liquid surface projection by Hasemann et al. [1], in the Mo-rich compositional region of the Mo-Si-B ternary system, Mo solid solution (Mo_{ss}) crystallized out first as the primary phase through the reaction of $L \rightarrow Mo_{ss}$. When the B content is high enough, a Mo_{ss} and Mo_2B mono-variant eutectic reaction occurs as $L \rightarrow Mo_{ss} + Mo_2B$. It is well known that TiC addition suppresses the Mo_2B formation in the as-cast microstructure of the Mo-Si-B (MoSiBTiC) alloy and instead generates Mo_2C [2]. The Mo_2C formation is shown in the lower Ti content region of the Mo-Ti-C ternary system [3]. Thus, it was considered that Ti and/or C generated by the decomposition of TiC changes the solidification sequence of the Mo-Si-B alloy. In contrast, ZrC addition to the Mo-Si-B alloy does not induce the formation of Mo_2C [4]. As a result, the ZrC-added Mo-Si-B (MoSiBZrC) alloy has the solidification sequence that the primary Mo_{ss} or ZrC and the secondary Mo_{ss} + ZrC eutectic. At the later stage of solidification, the MoSiBZrC alloy was shown to solidify along the solidification path of the Mo-Si-B alloy. This difference is expected from the lower solubility of ZrC in Mo, as shown in the Mo-Zr-C ternary system [5]. Cr is one of the critical elements that can improve the oxidation resistance of the Mo-Si-B alloy [6], and the Nb addition is expected to mitigate the embrittlement caused by the Cr addition. For theses reasons, in the present study, Cr and Nb were added to the MoSiBZrC alloy and the solidification path and phase equilibria were studied. The experimental results showed that the constituent phases of the as-cast MoSiBZrC alloy are Mo_{ss}, Mo_5SiB_2 (T_2), Mo_3Si and ZrC. The Cr addition formed the σ ($Cr_{0.36}Mo_{0.52}Si_{0.12}$) phase, but the Cr and Nb addition formed the $Mo_{0.26}Si_{0.25}Zr_{0.28}Cr_{0.1}Nb_{0.11}$ phase. The Mo_3Si phase disappeared in the as-cast Cr-added alloys. The solidification path of Mo-5Si-10B-5Zr-5C (mol %) alloy was Mo_{ss} (primary) $\rightarrow Mo_{ss}$ + ZrC $\rightarrow T_2 \rightarrow Mo_{ss} + T_2$ + ZrC $\rightarrow Mo_{ss} + Mo_3Si + T_2$ + ZrC. 20 at.% Cr addition changed the solidification path to ZrC (primary) $\rightarrow Mo_{ss}$ + ZrC $\rightarrow Mo_{ss} + T_2 \rightarrow Mo_{ss} + T_2$ + ZrC $\rightarrow \sigma$ + ZrC. The 5 at.% Nb addition changed the final solidification stage from the σ + ZrC to the $Mo_{ss} + Mo_{0.26}Si_{0.25}Zr_{0.28}Cr_{0.1}Nb_{0.11}$ eutectic. After annealing, the alloys were only composed of Mo_{ss}, T_2 and ZrC. The Cr addition increased the volume fraction of T_2 phase, and the Nb addition increased the volume fraction of ZrC phase. As a result, in the MoSiBZrC alloy, the Cr and Nb additions suppressed the Mo_3Si formation in the as-cast microstructure and changed the solidification sequence, but had not effect on the equilibrium phases.

References

[1] G. Hasemann et al., Mater. Desig., 2020, 185, 108233.
[2] H. Fukuyama et al., Sci. Rep. 9, 2019, 15049.
[3] S. Ida et al., High Tempe. Mater. Proce., 2020, 39 (1), 164-170.
[4] S. Nakayama et al., J. Japan Inst. Met. Mater., 2016, 80 (1), 92-101.
[5] C. Zhang et al., J. Phase Equilib. Diffus., 2018, 39, 766-777.
[6] S. Burk et al., JOM 63, 2011, 32–36.